# Generalized Wiener Estimation of Three-Dimensional Current Distribution from Biomagnetic Measurements

Kensuke Sekihara*, *Member, IEEE*, and Bernhard Scholz

*Abstract*—**This paper proposes a method for estimating three-dimensional (3–D) biocurrent distribution from spatio-temporal biomagnetic data. This method is based on the principle of generalized Wiener estimation, and it is formulated based on the assumption that current sources are uncorrelated. Computer simulation demonstrates that the proposed method can reconstruct a 3-D current distribution where the conventional least-squares minimum-norm method fails. The influence of noise is also simulated, and the results indicate that a signal-to-noise ratio of more than 20 for the uncorrelated sensor noise is needed to implement the proposed method. The calculated point spread function shows that the proposed method has very high spatial resolution compared to the conventional minimum norm method. The results of computer simulation of the distributed current sources are also presented, including cases where current sources are correlated. These results suggest that no serious errors arise if the source correlation is weak.**

## I. Introduction

THE inherent difficulty in the biomagnetic inverse problem is that a three-dimensional (3-D) current distribution must be estimated from a biomagnetic field measured on a two-dimensional (2-D) surface close to a human head or body. In such cases, the estimation is ill-posed. To reduce this ill-posedness, the current distribution to be estimated is often modeled by using the equivalent current dipole (ECD), which assumes a highly localized current source [1]. This ECD model has been applied to biomagnetic data having a relatively simple field pattern, such as evoked neuromagnetic fields generated from the primary sensory cortices. However, when the source current distribution is not localized, or when no information regarding the spatial extent of the source distribution is obtained, we cannot rely on ECD modeling.

One method has been developed that does not use a particular source model and, therefore, can estimate nonlocalized sources. This method seeks the current distribution that best fits the measured data with a minimum current norm. Thus, the method is often called the least-squares minimum-norm method [2]–[7]. This method has been successfully applied in 2-D cases where the biocurrent distribution is assumed to be confined to a single plane. Its 3-D application, however, poses a serious problem in that the signal current is estimated to be closer to the detector coils than its actual location [6], [7]. In some detector-coil and current-source configurations, the estimation error is so large that 3-D reconstruction by the minimum-norm method is almost meaningless. One such case will be simulated in Section III of this paper.

An approach that tries to avoid the above-mentioned problem involves adding a weighting term to the least-squares term [8]. This weighting term has small values for sources at a particular distance from the detectors and large values for sources at other distances. That is, the weight favors sources located at a particular distance from the detector coils, and such sources are chosen as a final solution. Accordingly, by controlling such a weight, we can select the distances of the sources. If we apply such a constraint to an actual cases, some information on source-detector distances is required *a priori*. Consequently, the applicability of such a method in actual cases is limited because it is usually difficult to obtain such information.

This paper presents a method that can provide 3-D reconstruction where the conventional minimum-norm method fails. It does not require any kind of prior information on the source-detector distances. It utilizes the principle of the generalized Wiener estimation with the assumption that the activities of the biocurrent sources are uncorrelated.

In this paper, following a brief summary of the conventional least-squares method, Section II describes the proposed method. Section III presents the results of computer simulation that show the method's effectiveness and limitations. Here, after demonstrating the method's 3-D capability, computer simulations regarding the influence of noise on the quality of the reconstructed results are performed. The method's point spread function is also calculated, and we explain how an appropriate pixel interval in the reconstruction can be select based on this calculated point spread function. Then, the results of computer simulation of the distributed current source reconstruction are presented, including cases where some correlation exists between the current sources. Section IV discusses the similarities and differences between the proposed method and other existing methods. Finally, Section V summarizes the results. Throughout this paper, lower-case italic letters in boldface represent vectors and upper-case italic letters in boldface represent matrices.

Manuscript received August 1, 1994; revised August 31, 1995. *Asterisk indicates corresponding author.*

*K. Sekihara is with the Central Research Laboratory, Hitachi, Ltd., P.O. Box 2, Kokubunji, Tokyo 185, Japan (e-mail: sekihara@crl.hitachi.co.jp).

S. Scholz is with Siemens AG, Medical Engineering Group, D-91 052 Erlangen, Germany.

Publisher Item Identifier S 0018-9294(96)01675-8.

## II. METHOD

### A. Problem Formulation

Let us define the magnetic field measured by the $m$th detector coil at time $t_k$ as $b_m(t_k)$, and a vector $\mathbf{b}(t_k) = (b_1(t_k), b_2(t_k), \cdots, b_M(t_k))^T$ as a set of measured data at time $t_k$, $k = 1, 2, \cdots, K$. Here, $M$ is the total number of detector coils, $K$ is the total number of time points, and the superscript $T$ indicates the matrix transpose. Let us also define the signal primary current distribution at time $t_k$ as a vector $\mathbf{f}(t_k) = (f_1(t_k), f_2(t_k), \cdots, f_{3N}(t_k))^T$. Here, $N$ is the total number of pixels and the $x$, $y$, and $z$ components of the primary current [9] located at the $i$th pixel are assigned to $f_{3(i-1)+1}(t_k)$, $f_{3(i-1)+2}(t_k)$, and $f_{3(i-1)+3}(t_k)$, respectively.

Next, we define the lead field matrix $\mathbf{L}$, which is a $M \times (3N)$ matrix. Its elements, $L_{m,3(i-1)+1}$, $L_{m,3(i-1)+2}$, and $L_{m,3(i-1)+3}$, represent the sensitivity of the $m$th detector to the $x$, $y$, and $z$ components of the primary current at the $i$th pixel. The column vector of the lead field matrix defined by $\mathbf{l}_p = (L_{1p}, L_{2p}, \cdots, L_{Mp})^T$ is introduced for later use. The lead field matrix is expressed using its column vectors as

$$\mathbf{L} = (\mathbf{l}_1, \mathbf{l}_2, \cdots, \mathbf{l}_{3N}). \tag{1}$$

Using the lead field matrix, the relationship between $\mathbf{b}(t_k)$ and $\mathbf{f}(t_k)$ is given by

$$\mathbf{b}(t_k) = \mathbf{L}\mathbf{f}(t_k) + \mathbf{n}(t_k) \tag{2}$$

where $\mathbf{n}(t_k)$ is the noise vector. The $m$th element of this noise vector is the noise contained in the $m$th detector measurement at time $t_k$. The problem that this paper deals with is how to find the optimum estimate of the signal primary current source distribution $\hat{\mathbf{f}}(t_k)$ at all time instants $k = 1, 2, \cdots, K$, from a given spatio-temporal data set of measured data $\mathbf{b}(t_k)$, $k = 1, 2, \cdots, K$.

### B. Least-Squares Minimum-Norm Estimation

The conventional method, called the least-squares minimum-norm method [2]–[7], solves this problem by minimizing the squared error between the measured and calculated magnetic field distributions at each time instant. That is, the current estimate $\hat{\mathbf{f}}(t_k)$ is obtained, at each time instant $t_k$, by minimizing the least squares cost function $\mathcal{F} = ||\mathbf{b}(t_k) - \hat{\mathbf{b}}(t_k)||^2$, where $\hat{\mathbf{b}}(t_k) = \mathbf{L}\hat{\mathbf{f}}(t_k)$. This minimization has a well-known solution using the Moore–Penrose generalized inverse $\mathbf{L}^-$ [10], namely

$$\hat{\mathbf{f}}(t_k) = \mathbf{L}^-\mathbf{b}(t_k). \tag{3}$$

Here, for underdetermined cases, $M < 3N$, $\mathbf{L}^-$ is given by $\mathbf{L}^- = \mathbf{L}^T(\mathbf{L}\mathbf{L}^T)^{-1}$.

This least-squares minimum-norm method has been successfully applied in 2-D cases where the biocurrent distribution is assumed to be confined to a single plane. Its 3-D application, however, poses a serious problem in that the location of the estimated source current is closer to the detector coils than its actual location [6], [7]. In some detector-source configurations, this reconstruction error affects the final results so seriously that 3-D reconstruction by this minimum-norm method is almost meaningless. Such a case will be shown in our computer simulations in the next section.

### C. Wiener Estimation

The method proposed in this paper utilizes the minimization of the following least-squares-error expressed in the source current space. That is, the cost function

$$\mathcal{F} = \sum_{k=1}^{K} ||\mathbf{f}(t_k) - \hat{\mathbf{f}}(t_k)||^2 \tag{4}$$

is minimized to obtain the optimum estimate $\hat{\mathbf{f}}(t_k)$. Here, $\mathbf{f}(t_k)$ is the true current distribution at time $t_k$, and the measured data $\mathbf{b}(t_k)$ is expressed as $\mathbf{b}(t_k) = \mathbf{L}\mathbf{f}(t_k)$. The solution which minimizes the above cost function is known to be the generalized Wiener estimate [11] or the minimum mean square error estimate [12]. This is expressed as

$$\hat{\mathbf{f}}(t_k) = \mathbf{S}\mathbf{L}^T\mathbf{D}^{-1}\mathbf{b}(t_k). \tag{5}$$

Here, defining the time average of $A$ as $\langle A \rangle$, $\mathbf{D}$ is the covariance matrix of the measured data defined as $\mathbf{D} = \langle \mathbf{b}(t_k)\mathbf{b}^T(t_k) \rangle$, and $\mathbf{S}$ is the covariance matrix of the signal current sources defined as $\mathbf{S} = \langle \mathbf{f}(t_k)\mathbf{f}^T(t_k) \rangle$.

When applying (5) to an actual problem, it is usually difficult to obtain an accurate estimate of the signal-source covariance matrix $\mathbf{S}$. One method for estimating $\mathbf{S}$ has been proposed by Smith [13] and independently by Sekihara *et al.* [14], [15]. In this method, the signal covariance matrix is estimated using the minimum-norm-based method. That is, the estimated signal covariance matrix $\hat{\mathbf{S}}$ is obtained from

$$\hat{\mathbf{S}} = \mathbf{L}^-(\mathbf{D} - \mathbf{C})(\mathbf{L}^-)^T \tag{6}$$

where $\mathbf{C}$ is the noise covariance matrix defined by $\mathbf{C} = \langle \mathbf{n}(t_k)\mathbf{n}^T(t_k) \rangle$. Substituting (6) into (5), we get

$$\hat{\mathbf{f}}(t_k) = \mathbf{L}^-(\mathbf{D} - \mathbf{C})\mathbf{D}^{-1}\mathbf{b}(t_k). \tag{7}$$

The Wiener method using the above equation provides a 2-D current reconstruction better than that obtained by the conventional minimum-norm method, when the signal-to-noise ratio of the measurements is low [15]. However, this method exhibits no improvements over the minimum-norm method when reconstructing 3-D current distributions, as will be shown by the computer simulations in the next section.

### D. Proposed Wiener Estimation

The Wiener method proposed in this paper estimates the signal covariance matrix in a different manner. Here, the signal current elements are assumed to be uncorrelated, i.e., all the nondiagonal elements of $\mathbf{S}$ are assumed to be zero. Then, estimating the signal covariance matrix is performed in the

following manner. Using the column vectors of the lead field matrix, let us rewrite (5) as

$$\hat{f}_p(t_k) = S_{pp}\mathbf{l}_p^T\mathbf{D}^{-1}\mathbf{b}(t_k) \tag{8}$$

where $S_{pp}$ is the $p$th diagonal element of the signal covariance matrix. Defining the estimate of $S_{pp}$ as $\hat{S}_{pp}$, we have

$$\begin{aligned}\hat{S}_{pp} &= \langle \hat{f}_p(t_k)\hat{f}_p(t_k)\rangle \\ &= \langle (S_{pp}\mathbf{l}_p^T\mathbf{D}^{-1}\mathbf{b}(t_k))(S_{pp}\mathbf{l}_p^T\mathbf{D}^{-1}\mathbf{b}(t_k))^T\rangle \\ &= S_{pp}^2\mathbf{l}_p^T\mathbf{D}^{-1}\mathbf{l}_p.\end{aligned}$$

Assuming that $\hat{S}_{pp} = S_{pp}$, one can obtain the relationship $\hat{S}_{pp} = 1/(\mathbf{l}_p^T\mathbf{D}^{-1}\mathbf{l}_p)$. Thus, the proposed Wiener estimation becomes

$$\hat{f}_p(t_k) = \frac{\mathbf{l}_p^T\mathbf{D}^{-1}\mathbf{b}(t_k)}{\mathbf{l}_p^T\mathbf{D}^{-1}\mathbf{l}_p}. \tag{9}$$

It should be pointed out that no pixel discretization of the reconstruction volume is needed for this method. That is, the current elements at an arbitrary point $\mathbf{x}$ can be reconstructed. Here, $\mathbf{x}$ is equal to $(x, y, z)$ where $x$, $y$, and $z$ are the continuous spatial coordinates. Let us define $j_\xi(\mathbf{x}, t_k)$ as the $\xi$ component of the current density at $\mathbf{x}$ and at time $t_k$, where $\xi$ is equal to either $x$, $y$, or $z$. Let us also define $\tilde{\mathbf{b}}(\xi, \mathbf{x})$ as the forward solution calculated by assuming the $\xi$ unit component of the current element is located at $\mathbf{x}$. Using this $\tilde{\mathbf{b}}(\xi, \mathbf{x})$, the estimate of the current component $\hat{j}_\xi(\mathbf{x}, t_k)$ is given by

$$\hat{j}_\xi(\mathbf{x}, t_k) = \frac{\tilde{\mathbf{b}}^T(\xi, \mathbf{x})\mathbf{D}^{-1}\mathbf{b}(t_k)}{\tilde{\mathbf{b}}^T(\xi, \mathbf{x})\mathbf{D}^{-1}\tilde{\mathbf{b}}(\xi, \mathbf{x})}. \tag{10}$$

The only difference between this equation and (9) is the replacement of $\mathbf{l}_p$ with $\tilde{\mathbf{b}}(\xi, \mathbf{x})$. Considering that $\mathbf{l}_p$ is the forward solution of the $p$th unit current element, it is easy to see that this equation is the natural extension of (9) to its continuous form. The current density at an arbitrary location can be reconstructed using (10). Note that (9) and (10) give dimensionless values and, thus, relative values of a current source distribution can be reconstructed using these equations.

## III. Computer Simulations

### A. General

Computer simulations were performed to show the effectiveness and limitations of the proposed method. A magnetometer with 37 channels, each having a first-order gradiometer coil with a 7.1-cm baseline, was assumed in these simulations. The gradiometer coils are hexagonally aligned on a plane defined as a $x$-$y$ plane having its origin at the center of the hexagon. The detector coil alignment is shown in Fig. 1. This alignment simulates the KRENIKON™ biomagnetic measurement system [16]. The $z$ direction is defined as the direction perpendicular to the detector-coil-aligned plane, and the $z$ coordinate is zero at this plane. The values of the spatial coordinates $(x, y, z)$ are expressed in centimeters. The horizontally layered infinite half-space conductor model [9] is assumed for ease in calculation, and the boundary of the conductor is assumed to be perpendicular to the $z$ axis. Thus, only the $x$ and $y$ components of the primary current vectors are magnetically effective and their $z$ components are assumed to be zero.

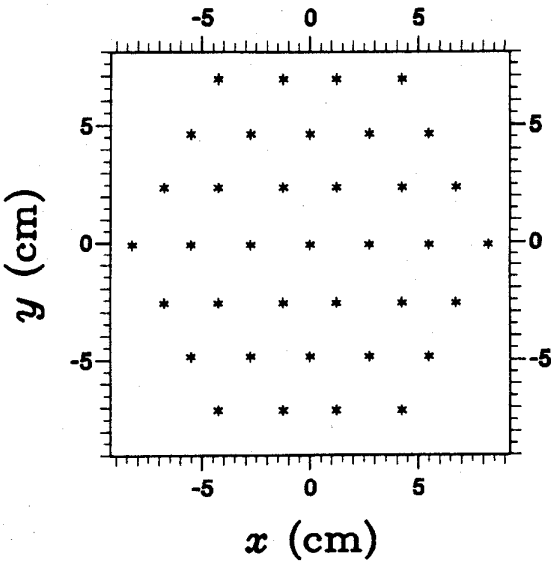


Fig. 1. Detector coil alignment assumed in the computer simulation. The asterisks indicate the coil locations. This alignment simulates the KRENIKON™ biomagnetic measurement system [16].

### B. Three-Dimensional Reconstruction

The 3-D reconstruction capability of the proposed method is first demonstrated by comparing it with the other two methods described in Section II. Two time-varying magnetic-field sources are assumed to exist: the first source at $(-4, 1, -3)$ and the second source at $(3, 1, -5)$. The $x$ and $y$ components of those sources randomly fluctuate around a zero average and their root-mean-square (rms) values equal 20 nAm. Here, the activities of the two sources are assumed to be uncorrelated with each other.

Let us choose the time instant at which the $x$ component of the first source and the $y$ component of the second source each happen to equal 20 nAm, and the other component of each source is zero. The source and detector configuration at this instant is depicted in Fig. 2. The magnetic field data at this instant is obtained by subtracting the field strength at the gradiometer's upper-coil position from that at the lower-coil position. The simulated measured data is obtained by adding uncorrelated Gaussian noise with a standard deviation of 20 femto Tesla (fT) to the magnetic field data. This Gaussian noise simulates the sensor noise, which is the noise generated from the SQUID's and the electronics associated with them. The signal-to-noise ratio (SNR) of this simulated data is approximately 20. The SNR is defined by the ratio of the average intensity of the signal magnetic field to the standard deviation of the noise.

The reconstruction experiments are performed using the three methods described in Section II. Here, the reconstruction volume covers $-8 \le x \le 8$, $-8 \le y \le 8$, and $-1 \le z \le -9$.

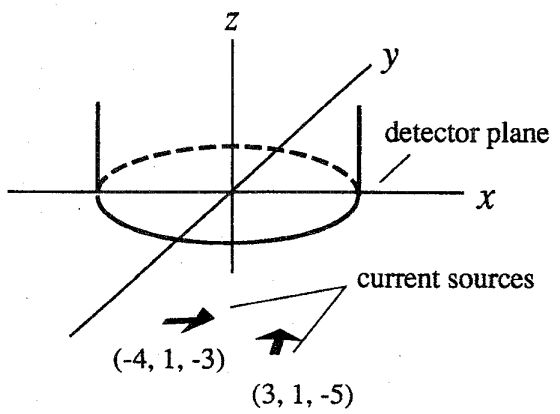


Fig. 2. Schematic view of the source and detector configuration assumed in the computer simulation. Current sources exist at $(-4, 1, -3)$ and $(3, 1, -5)$.

It consists of $17 \times 17 \times 9$ pixels. Note that each location of the two sources are set at the center of a pixel in this computer simulation to avoid unnecessary complexity in the interpretation of the reconstructed results. The problem that arises when a source is not located at a pixel center, as well as the choice of pixel intervals to avoid this problem, are discussed in Section III-E. An example of erroneous results is also shown; these results were obtained because a source was not located at a pixel center and an inappropriately large pixel interval was used. Distortion-free reconstruction results for sources not necessarily located at pixel centers are shown in Section III-F.

First, conventional minimum-norm reconstruction was performed using this measured field data. The results obtained using (3) are shown in Fig. 3. It should be mentioned that, in this computer simulation, no regularization technique of any kind was needed to calculate the generalized inverse in (3). This is because the condition number of $\mathbf{L}\mathbf{L}^T$, defined by the ratio of its largest singular value to the smallest, is small and nearly equal to 5.4. Fig. 3 displays the reconstructed current sources on planes equal to $z = -1$, $z = -3$, $z = -5$, and $z = -7$. Here, the arrows represent the relative values of the reconstructed current sources, and the largest arrow represents the largest source vector in the 3-D reconstruction.

In these results, only the uppermost plane, the plane closest to the detector-aligned plane, contains current elements of significantly large intensity, while sources in the other planes are almost negligible. Even in the uppermost plane, only the source closest to the detectors is reconstructed. These results clearly show that the minimum-norm method provides severely distorted 3-D reconstruction in this case.

Next, the covariance matrix of the measured data $\mathbf{D}$ was estimated from 1000 data generations; all generated data contains the simulated sensor noise with the same standard deviation described above. The $(\ell, m)$ element of the covariance matrix, $D_{\ell m}$, is calculated using $D_{\ell m} = \frac{1}{K}\sum_{k=1}^{K} b_\ell(t_k) b_m(t_k)$. Here, $b_\ell(t_k)$ is the magnetic field measured by the $\ell$th channel at the $k$th data generation, and $K$ is equal to 1000. This simulates data acquisition for 1 s with a sampling interval of 1 ms.

The previously proposed Wiener reconstruction, which uses (7), was applied to the same magnetic field data. The reconstruction results, almost identical to those shown in Fig. 3, are shown in Fig. 4. These results show that, in terms of 3-D reconstruction capability, the previously proposed Wiener method using (7) provides no improvement over the minimum-norm method.

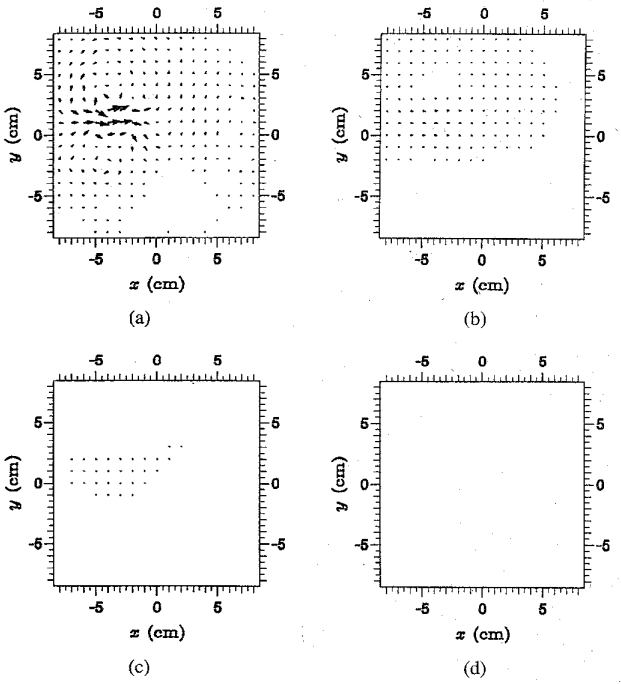


Fig. 3. Results of 3-D reconstruction by the least-squares minimum-norm method. Equation (3) was used, and the SNR of the data is 20. The planes equal to (a) $z = -1$, (b) $z = -3$, (c) $z = -5$, and (d) $z = -7$ are displayed. The arrows represent the relative values of the reconstructed current sources, and the largest arrow represents the largest source vector in the 3-D reconstruction.

Finally, the proposed Wiener reconstruction using (9) was applied with the data covariance matrix $\mathbf{D}$ obtained above. The results are shown in Fig. 5. Here, both sources are reconstructed, clearly demonstrating this method's 3-D reconstruction capability.

### C. Influence of Uncorrelated Sensor Noise

In biomagnetic measurements, noise may be caused either internally or externally. Internal noise is caused in SQUID's and receiver electronics, and it is spatially uncorrelated. The simulated measured data used in the preceding section was assumed to have an SNR for this sensor noise equal to 20. In actual measurements, the SNR may sometimes be lower than this value, and have values ranging from five to 10, depending on the number of averaging. In this subsection, the proposed method is tested for data with lower SNR's to determine the method's tolerance to low SNR. Two sets of simulated measured data were generated in exactly the same manner as described in Section III-B, except we assumed that the standard deviation of sensor noise is equal to 40 fT and 80 fT. This results in SNR's of these data sets equal to 10 and five, respectively. Results of the reconstruction using (9) with these data sets are shown in Figs. 6 and 7.

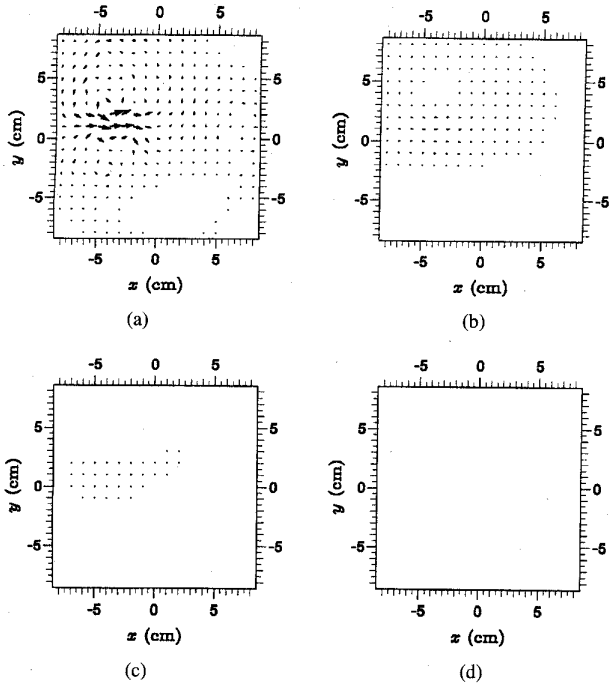


Fig. 4. Results of 3-D reconstruction by the previously proposed Wiener method. Equation (7) was used and the SNR of the data is 20. The planes equal to (a) $z = -1$, (b) $z = -3$, (c) $z = -5$, and (d) $z = -7$ are displayed.

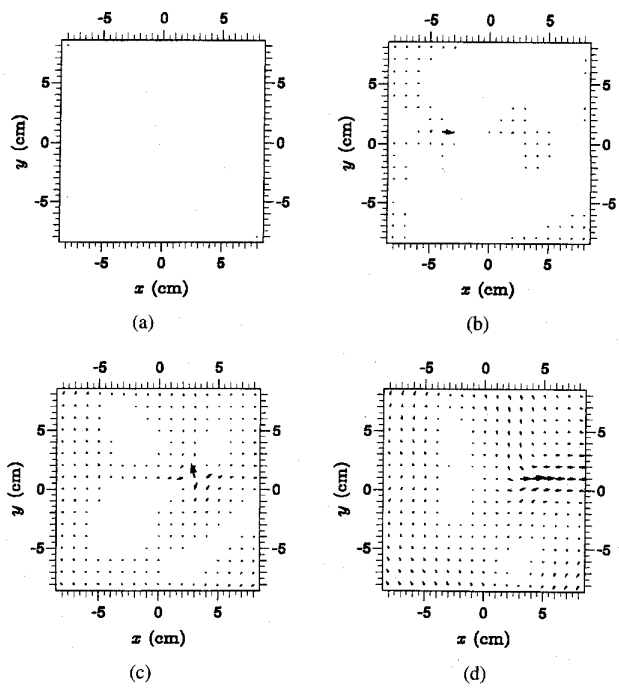


Fig. 6. Results of applying the proposed Wiener method to data with SNR equal to 10. The reconstructed planes equal to (a) $z = -1$, (b) $z = -3$, (c) $z = -5$, and (d) $z = -7$ are shown.

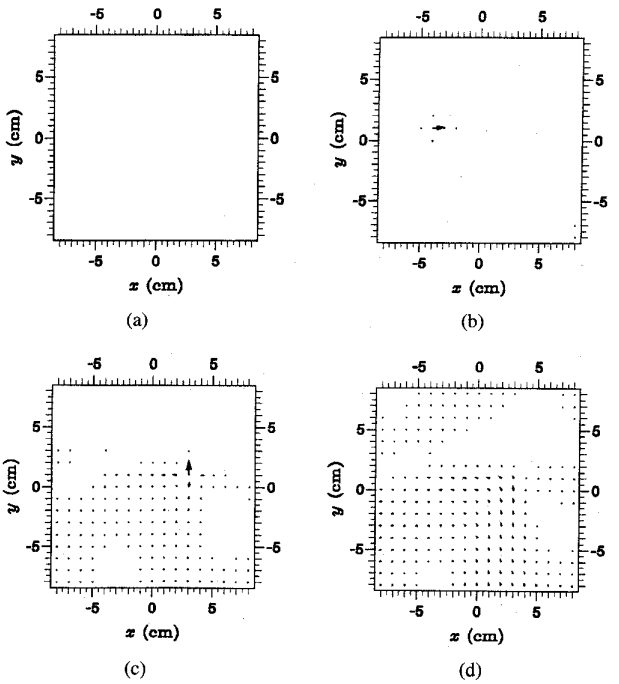


Fig. 5. Results of 3-D reconstruction by the newly proposed Wiener method. Equation (9) was used, and the SNR of the data is 20. The planes equal to (a) $z = -1$, (b) $z = -3$, (c) $z = -5$, and (d) $z = -7$ are displayed.

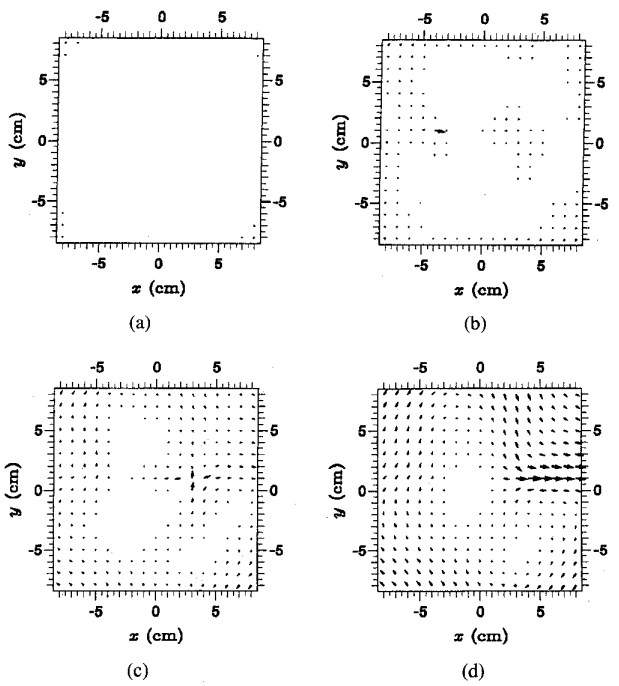


Fig. 7. Results of applying the proposed Wiener method to data with SNR equal to 5. The reconstructed planes equal to (a) $z = -1$, (b) $z = -3$, (c) $z = -5$, and (d) $z = -7$ are shown.

The results from the data with SNR of 10 are shown in Fig. 6 where the two current sources are clearly reconstructed but large artifacts appear in the plane $z = -7$. In Fig. 7, which shows the results from the data whose SNR is equal to five, the intensities of the two sources are considerably distorted and the artifacts appearing in the $z = -7$ plane are more

pronounced. These results indicate that the results obtained using the proposed method may contain errors unless the SNR for the sensor noise is quite high. An SNR of more than 20 is needed for the source and detector configuration assumed in our computer simulation. This point will be further discussed in Section IV.

### *D. Influence of Correlated Noise*

The biomagnetic data often contains spatially correlated noise caused by external noise sources. Especially, in neuromagnetic measurements, the measured data is sometimes considerably influenced by noise magnetic fields caused by spontaneous brain activities not related to the neural activities under study [17], [18]. The influence of such correlated noise is different from that of uncorrelated sensor noise discussed in Section III-C. That is, since the proposed Wiener estimation cannot discriminate signal sources from noise sources, it reconstructs noise sources as well as signal sources. Reconstruction results are generally not affected by the noise sources when the signal sources are well separated from the noise sources. However, when strong noise sources are located near a signal source, reconstruction results can be affected.

This situation is simulated in Fig. 8. Here, a fluctuating noise source whose rms value is equal to 200 nAm is assumed to exist at $(-3, -2, -10)$ in addition to the two signal sources. Note that the noise source is 10 times stronger than the signal sources. The SNR for this external noise field is equal to 1.3. This SNR is defined by the ratio of the average intensity of the signal magnetic field to that of the noise magnetic field. Here, a sensor noise of 20 fT is assumed, and the SNR for this sensor noise is 20. The results in Fig. 8 show that, although the two signal sources are clearly reconstructed, the $z = -7$ plane contains strong ghost artifacts caused by the noise source. The generation of these ghost artifacts can be understood through an investigation of the spatial resolution in the $z$ direction for deep sources. This investigation is presented in the next section.

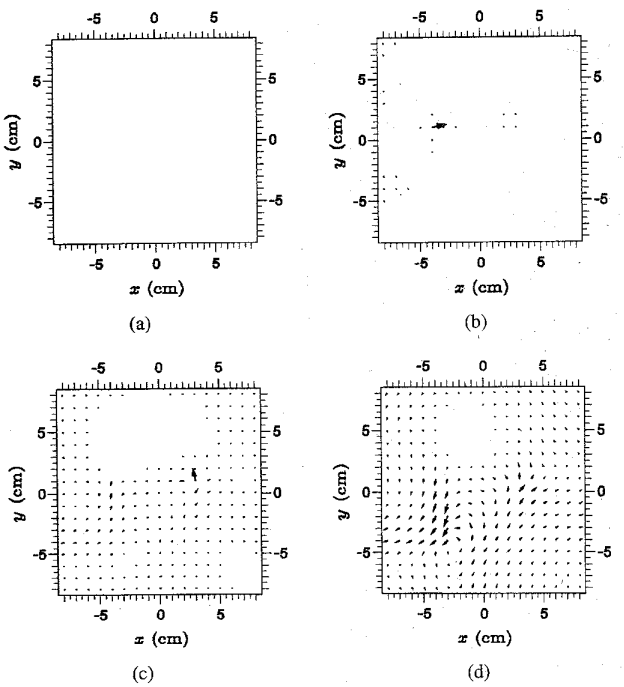


Fig. 8. Influence of a strong noise source on the reconstructed results. In addition to the two signal sources, a fluctuating noise source whose rms value is 10 times stronger than the signal sources is assumed to exist at $(-3, -2, -10)$. The reconstructed planes equal to (a) $z = -1$, (b) $z = -3$, (c) $z = -5$, and (d) $z = -7$ are shown.

### *E. Point-Spread Function*

Let us assume that a current source with the unit $\xi$ component is located at $\mathbf{x}_0$ where $\xi$ indicates $x$ or $y$. We define the $\xi$ component of the estimated current source at $\mathbf{x}$ as $Q_\xi(\mathbf{x}, \mathbf{x}_0)$. Then, $Q_\xi(\mathbf{x}, \mathbf{x}_0)$ can be obtained from

$$Q_\xi(\mathbf{x}, \mathbf{x}_0) = \frac{\tilde{\mathbf{b}}^T(\xi, \mathbf{x})\mathbf{D}^{-1}\tilde{\mathbf{b}}(\xi, \mathbf{x}_0)}{\tilde{\mathbf{b}}^T(\xi, \mathbf{x})\mathbf{D}^{-1}\tilde{\mathbf{b}}(\xi, \mathbf{x})} \tag{11}$$

where $\tilde{\mathbf{b}}(\xi, \mathbf{x})$ indicates the forward solution created by a source with the unit $\xi$ component at $\mathbf{x}$. This $Q_\xi(\mathbf{x}, \mathbf{x}_0)$ represents the point spread function (PSF) of the proposed method, and it expresses the spatial resolution of the proposed method at $\mathbf{x}_0$.

The PSF for $\xi = y$ and $\mathbf{x}_0 = (0, 0, -5)$ are plotted in Fig. 9(a) and (b). Here, to calculate $\mathbf{D}$, 1000 data generations were performed by assuming a current source at $\mathbf{x}_0$ and, in each generation, the uncorrelated sensor noise was added to set the SNR equal to 20. The plots of the PSF obtained by the least-squares minimum norm reconstruction are also shown in Fig. 9(c) and (d). The PSF obtained by the proposed method has a sharp peak, indicating the method's high spatial resolution. Conversely, the PSF obtained using the minimum-norm method has a very blurred peak in the $x$-$y$ plane, and does not even have a peak in the $z$ direction. This shape of the PSF in the $z$ direction again suggests that the sources estimated by the minimum-norm method appear too close to the detector plane.

The cross sections of the PSF of the proposed method in the $x$, $y$, and $z$ directions for sources with four different $z$ locations are shown in Fig. 10. According to this figure, the resolution is influenced by the distance of the source from the detectors. The resolution in the $z$ direction is poorer than in the other two directions, especially for sources far from the detectors in the $z$ direction, i.e., for deep sources. These results indicate that if a large noise source exists far in the $z$ direction and if the plane just above this noise source is reconstructed, ghost artifacts are likely to appear due to the noise source in the reconstructed plane. This is simulated in Fig. 8.

The plots shown in Fig. 10 are useful for determining the appropriate pixel interval in a reconstruction region. The reconstructed results shown in Figs. 5–8 use pixel intervals of 0.5 cm in the $x$ and $y$ directions. Since the full width at half maximum (FWHM) of the PSF in the $x$ or $y$ direction is less than 0.1 cm for the plane $z = -3$, this 0.5-cm pixel interval is too large for the first source located in the $z = -3$ plane. Thus, if this source was located between pixel points, it might not be reconstructed.

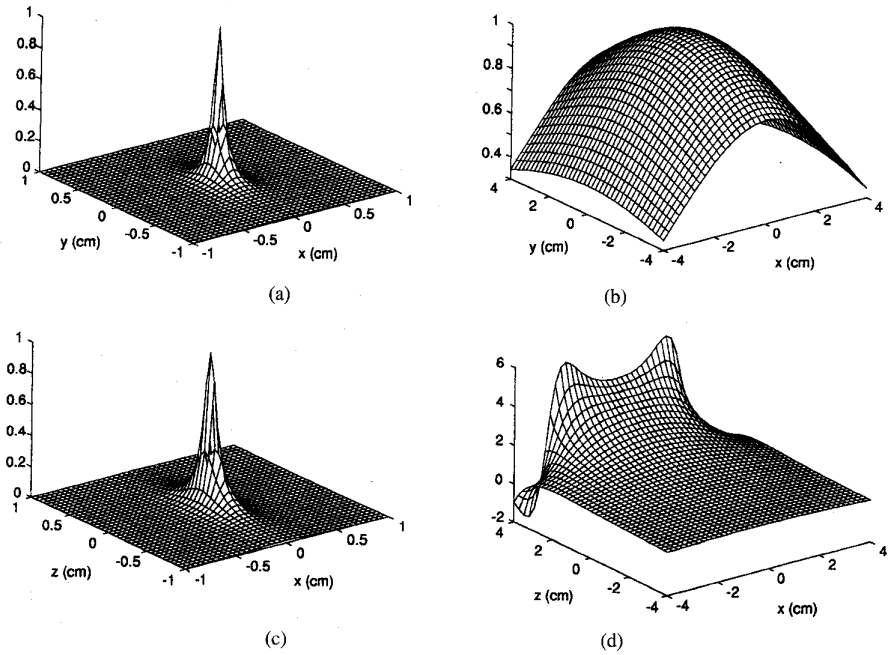


Fig. 9. Point spread function of the proposed Wiener method for a source located at $(0,\ 0,\ -5)$: (a) the $x$-$y$ plane and (b) the $x$-$z$ plane. Point spread function of the least-squares minimum norm method for the same source: (c) the $x$-$y$ plane and (d) the $x$-$z$ plane. The origins of these four plots are all equal to $(0, 0, -5)$.

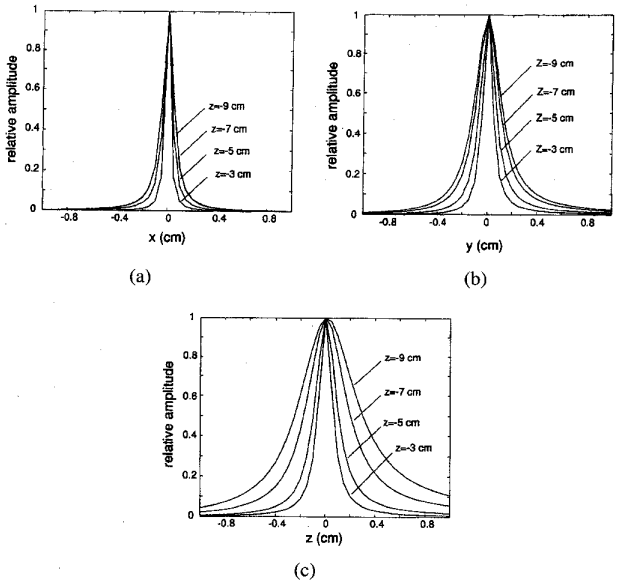


Fig. 10. Cross-sectional view of the point spread function for a source located at $(0, 0, z)$ where $z = -3, -5, -7$, and $-9$. Cross-sections are with respect to (a) the $x$ direction, (b) the $y$ direction, and (c) the $z$ direction.

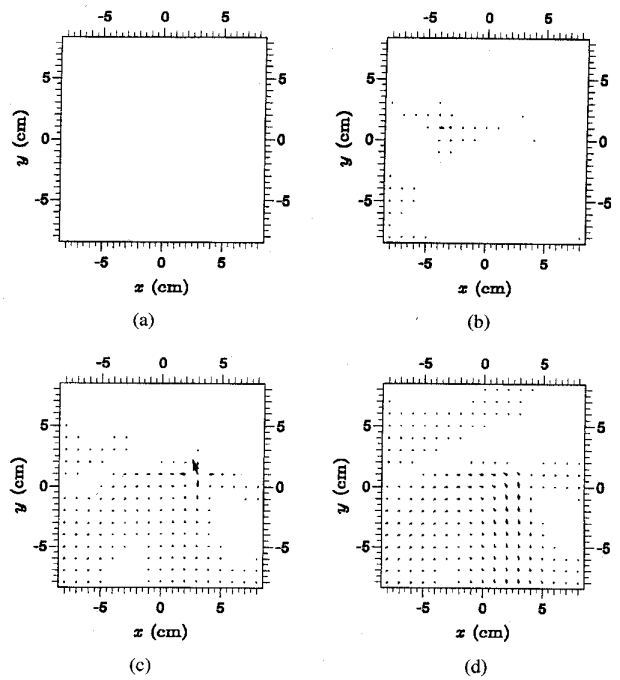


Fig. 11. Results of the experiments with two sources when one source is not located at a pixel center and the pixel interval is set to be much larger than the FWHM of the PSF. The first source is located at $(-4, 1.3, -3)$, and the pixel interval is set at 0.5 cm. Results when the source is located at the pixel center $(-4, 1, -3)$ are shown in Fig. 5.

This is simulated in Fig. 11. In this simulation, the simulated data is generated by assuming exactly the same conditions as for the results in Fig. 5 except that the first source is located at $(-4, 1.3, -3)$ instead of $(-4, 1, -3)$. The pixel interval remains to be 0.5 cm. In Fig. 11, the intensity of this source is greatly reduced because the source was located away from a pixel center and the pixel interval is much larger than the FWHM of the PSF. Thus, before reconstructing unknown sources, one should first determine an appropriate pixel interval by calculating the FWHM of the PSF to avoid erroneous reconstruction results such as those shown in Fig. 11. In the computer simulation in the next section, distributed sources are

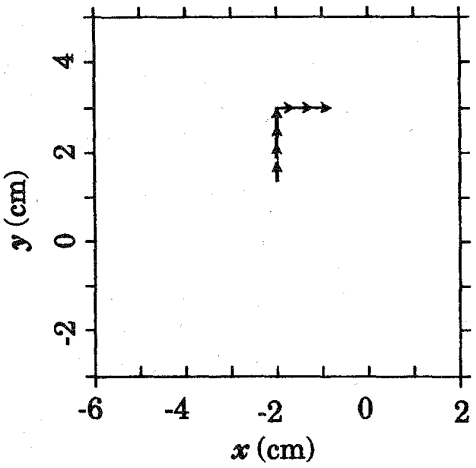


Fig. 12. The configuration of the current source cluster used for the distributed source reconstruction experiment.

reconstructed with a pixel interval nearly equal to the FWHM of the PSF.

### *F. Distributed Source Reconstruction and Influence of Source Correlation*

In this section, the proposed method's capability for reconstructing distributed current sources is tested. Here cluster of seven current sources located 0.5 cm apart are used as distributed current sources. All sources are located in a plane equal to $z = -5$, and the $x$ and $y$ coordinates of the seven sources are $(-2, 1)$, $(-2, 1.5)$, $(-2, 2)$, $(-2, 2.5)$, $(-2, 3)$, $(-1.5, 3)$, and $(-1, 3)$. Here, each source randomly fluctuates with the rms value equal to 10 nAm. We, at first, assume that the fluctuations of these sources are uncorrelated with each other. One thousand data generations are performed to calculate the covariance matrix. In each data generation, Gaussian noise equal to 20 fT is added to set the SNR of the simulated measured data to approximately 20.

The time point at which seven sources happen to have current moments equal to $(0, 10)$, $(0, 10)$, $(0, 10)$, $(0, 10)$, $(10, 0)$, $(10, 0)$, and $(10, 0)$ nAm was chosen for the reconstruction. This source configuration is depicted in Fig. 12. Results of the reconstruction at this time point are shown in Fig. 13. Here, the planes equal to $z = -3$, $z = -5$, and $z = -7$ are reconstructed. The pixel interval is set equal to 0.2 cm, according to the FWHM of the PSF for $z = -5$. Each plane covers $-6 \leq x \leq 2$ and $-3 \leq y \leq 5$, and $41 \times 41$ pixels are contained in these planes. Note that the positions of the sources are not always equal to the centers of the pixels in this case. In Fig. 13, the cluster of the sources are clearly reconstructed, and no artifacts are observed.

Up to this point, our computer simulation assumes that the activities of current sources are uncorrelated. However, this assumption may not always be valid in biomagnetic measurement. There have been several reports that suggest the existence of correlated neural activities in a human brain [19]–[21]. The distributed current sources therefore are likely to have some correlation with each other. Next, we evaluate

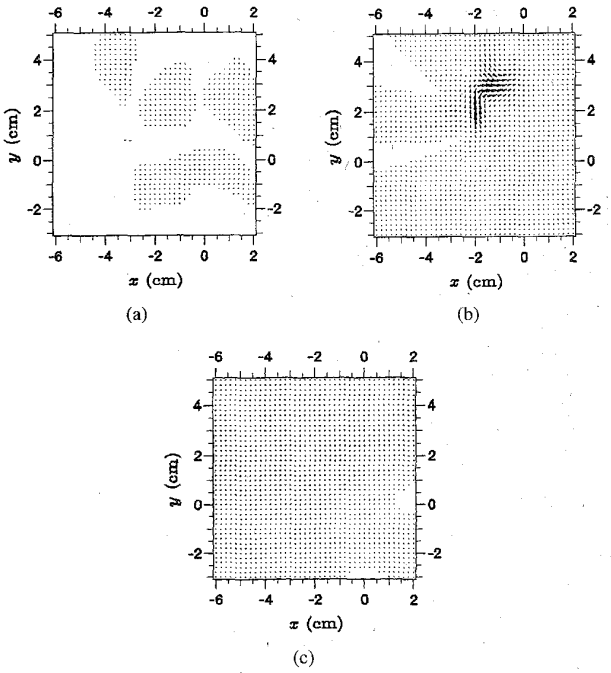


Fig. 13. Results of distributed source reconstruction experiments. The configuration of the current sources are shown in Fig. 12, and the activities of these sources are uncorrelated. Reconstructed planes equal to (a) $z = -3$, (b) $z = -5$, and (c) $z = -7$ are shown, and each contains $41 \times 41$ pixels, resulting in the pixel interval equal to 0.2 cm.

the method's tolerance to source correlation using the same distributed source model.

Let us define the $i$th source moment as $(q_x^i, q_y^i)$. To calculate correlated current sources, 16 Gaussian random numbers with an rms value of 10 nAmm are calculated in each of the 1000 data generations. They are denoted as $r_A$, $r_B$, and $r_1, r_2, \cdots, r_{14}$. The moment of the $i$th source is calculated as $q_x^i = \alpha r_A + (1 - \alpha) r_{2i-1}$ and $q_x^i = \alpha r_B + (1 - \alpha) r_{2i}$, where the parameter $\alpha$ controls the mutual correlation among the moment components of the sources. The mutual correlation for $\mu$th and $\nu$th sources is defined as

$$\beta = \langle q_\xi^\mu q_\xi^\nu \rangle \Big/ \sqrt{\langle (q_\xi^\mu)^2 \rangle \langle (q_\xi^\nu)^2 \rangle} \tag{12}$$

where $\langle A \rangle$ indicates the average of $A$ over 1000 data generations, and $\xi$ indicates $x$ or $y$.

Two sets of 1000 data points whose mutual correlation $\beta$ is equal to 0.3 and 0.7 were generated, and the covariance matrices calculated using these data sets. The same magnetic field data whose reconstruction is shown in Fig. 13 was again reconstructed using those covariance matrices. The results are shown in Fig. 14 for the case of $\beta = 0.3$ and in Fig. 15 for the case of $\beta = 0.7$. In Fig. 14, the sources are reconstructed without any serious artifacts, although a small amount of distortion is contained in the results. In Fig. 15, however, the reconstructed source cluster is considerably distorted. These results suggest that when the source correlation is weak, the proposed method can reconstruct distributed sources without any serious artifacts, but the reconstruction results may contain severe errors when the strong source correlation exists.

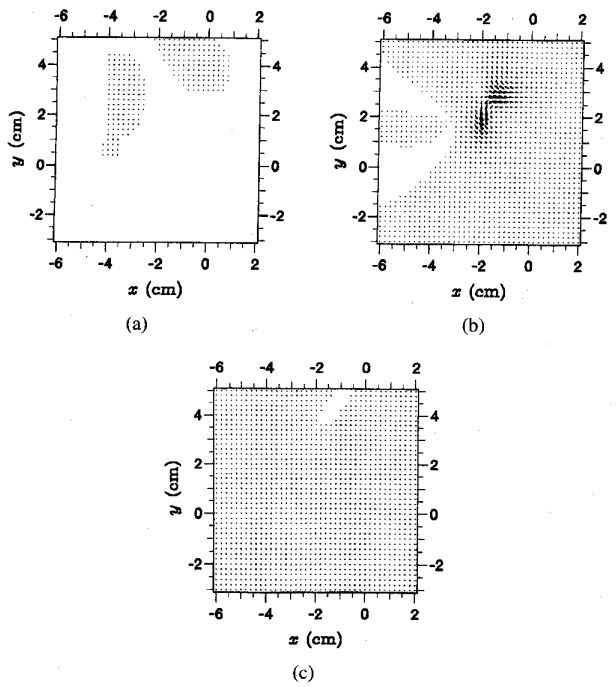


Fig. 14. Results of distributed source reconstruction experiments for weakly correlated sources. The mutual correlation defined by (12) is 0.3. Reconstructed planes equal to (a) $z = -3$, (b) $z = -5$, and (c) $z = -7$, are shown.

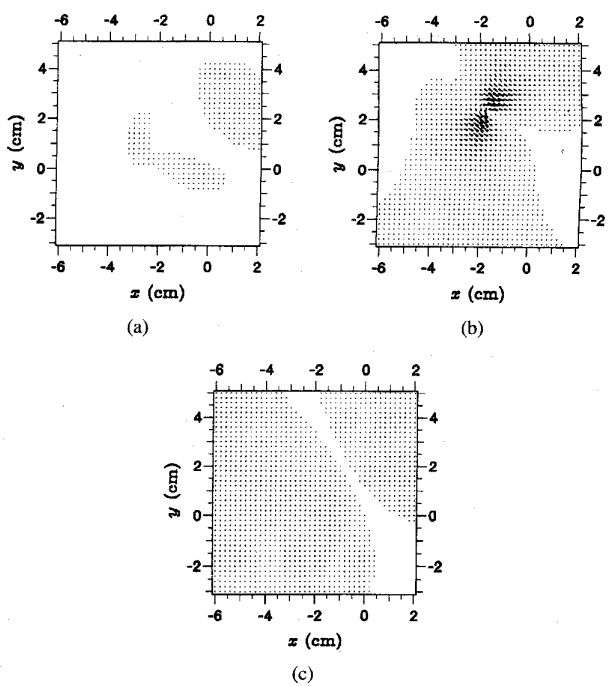


Fig. 15. Results of distributed source reconstruction experiments for strongly correlated sources. The mutual correlation defined by (12) is 0.7. Reconstructed planes equal to (a) $z = -3$, (b) $z = -5$, and (c) $z = -7$ are shown.

## IV. Discussions

According to the computer simulation in Section III-C, the SNR for the internal sensor noise must be over 20 to implement the proposed method. The achievement of such a high SNR in neuromagnetic measurements, however, may be difficult at present. Recently, though, the development of SQUID biomagnetometers with sensor noise of 2 to 5 fT/$\sqrt{\text{Hz}}$ has been reported [22]–[24]. If we assume a 100-Hz bandwidth, these noise values correspond to the incident magnetic field intensity equal to 20 to 50 fT. Typical intensities of neuromagnetic fields range from 1 pT for alpha rhythm to 100 fT for evoked fields [25]. For measurements of an evoked field, the SNR for the sensor noise can be improved by signal averaging: for example, the SNR can be improved ten-fold by 100-times averaging. Thus, it will not be that difficult to achieve an SNR of 20 if such a magnetometer is used.

The proposed method may not work well when the SNR of the uncorrelated sensor noise is extremely high. This is because the data covariance matrix $\mathbf{D}$ becomes nearly singular in such cases, and $\mathbf{D}^{-1}$ cannot be calculated. This fact usually does not affect the practical application of the method because in most cases of biomagnetic measurements the SNR of the sensor noise seldom exceeds 50. However, if the method is applied to extremely high SNR data, one should be careful about interpreting the results.

In the method proposed in this paper, (9) and (10) are derived by ignoring any source correlation. When correlation among the current sources is so strong that it must be taken into account, i.e., when the off-diagonal terms of the signal covariance matrix cannot be ignored, the reconstructed results obtained using (9) contain distortion as shown in our computer simulation. The equation that the signal source covariance matrix $\mathbf{S}$ generally must satisfy can be derived in a manner similar to the derivation of (9). That is, using (5) and omitting the explicit time notation $t_k$ for simplicity, we obtain

$$\begin{aligned}\mathbf{S} &= \langle \mathbf{f}\mathbf{f}^T \rangle \\ &= \mathbf{S}\mathbf{L}^T\mathbf{D}^{-1}\langle \mathbf{b}\mathbf{b}^T \rangle (\mathbf{S}\mathbf{L}^T\mathbf{D}^{-1})^T = \mathbf{S}(\mathbf{L}^T\mathbf{D}^{-1}\mathbf{L})\mathbf{S}. \end{aligned} \quad (13)$$

This equation indicates the relationship

$$\mathbf{S}^+ = (\mathbf{L}^T\mathbf{D}^{-1}\mathbf{L}) \quad (14)$$

where $\mathbf{S}^+$ is the conditional pseudo-inverse matrix of $\mathbf{S}$ [11]. Unfortunately, this conditional pseudo-inverse matrix is not uniquely determined, and it is impossible to further estimate $\mathbf{S}$ from (14). However, if some kinds of prior information can be utilized, a reasonable estimate of $\mathbf{S}$ may be obtained using (14).

Our computer simulation shows that a reconstruction nearly free from serious errors can be obtained even using (9), if the correlation is relatively small. In our computer simulation, acceptable results can be obtained when the relative source correlation coefficient defined by (12) is equal to 0.3. This value, however, depends on the source and detector configurations, and cannot be generalized to be valid in all cases. Thus, the method's tolerance to source correlation must be more completely evaluated through applying it to many cases of actual biomagnetic measurements.

It must be pointed out that (9) is basically the same as Capon's method originally proposed in seismic data processing to obtain high resolution power spectral density estimates

[26]. In this Capon's method, one seeks the weight $\mathbf{w}(p) = (w_1(p), w_2(p), \cdots, w_M(p))^T$ which gives the estimate $\hat{f}_p(t_k)$ using the linear relationship $\hat{f}_p(t_k) = \mathbf{w}^T(p)\mathbf{b}(t_k)$. The weight $\mathbf{w}(p)$ is determined in such a way that it minimizes the second term on the right-hand side of the following equation:

$$\hat{f}_p(t_k) = \mathbf{w}^T(p)\mathbf{l}_p f_p(t_k) + \sum_{q \neq p} \mathbf{w}^T(p)\mathbf{l}_q f_q(t_k). \quad (15)$$

It is easy to show that the solution of this minimization is equal to $\mathbf{w}^T(p) = (\mathbf{l}_p^T\mathbf{D}^{-1})/(\mathbf{l}_p^T\mathbf{D}^{-1}\mathbf{l}_p)$. The estimation derived from this weight is equal to that derived from (9). In this Capon's derivation, it is not easy to see that the assumption that the sources are uncorrelated is implicitly imposed. On the other hand, in our derivation described in Section II-D, since (9) is formulated as a special case of the Wiener estimation, the assumption made to derive this equation is much clearly understood.

It is interesting to point out a similarity between the proposed Wiener reconstruction and the multiple dipole estimation using the MUSIC (MUltiple SIgnal Classification) algorithm [27], [28]. This algorithm uses the idea of the noise and the signal subspaces. The signal subspace denoted by $\mathbf{E}_S$ is the space spanned by the eigenvectors corresponding to the signal eigenvalues of $\mathbf{D}$, and the noise subspace denoted by $\mathbf{E}_N$ is the space spanned by the eigenvectors corresponding to the noise eigenvalues of $\mathbf{D}$. The original MUSIC algorithm [27] calculates the MUSIC metric defined by $J(p) = 1/(\mathbf{l}_p^T\mathbf{E}_N\mathbf{E}_N^T\mathbf{l}_p)$ at all voxel locations, and chooses points where the metric has maxima as the estimated locations of signal sources.

In our method, the time-averaged squared intensity is calculated from $S_{pp} = 1/(\mathbf{l}_p^T\mathbf{D}^{-1}\mathbf{l}_p)$. The eigendecomposition of the matrix $\mathbf{D}^{-1}$ can be expressed as $\mathbf{D}^{-1} = \mathbf{E}_S\Lambda_S^{-1}\mathbf{E}_S^T + \mathbf{E}_N\Lambda_N^{-1}\mathbf{E}_N^T$ where $\Lambda_S$ and $\Lambda_N$ are the signal and noise eigenmatrices of $\mathbf{D}$. When the noise is uncorrelated, with its variance equal to $\sigma^2$, we have the relationship

$$\mathbf{l}_p^T\mathbf{D}^{-1}\mathbf{l}_p = \mathbf{l}_p^T\mathbf{E}_S\Lambda_S^{-1}\mathbf{E}_S^T\mathbf{l}_p + \frac{1}{\sigma^2}\mathbf{l}_p^T\mathbf{E}_N\mathbf{E}_N^T\mathbf{l}_p. \quad (16)$$

When the signal source consists of a few localized sources, namely a few current dipoles, the first term on the right-hand side of this equation is significantly smaller than the second term and can therefore be neglected. Thus

$$\mathbf{l}_p^T\mathbf{D}^{-1}\mathbf{l}_p \sim \frac{1}{\sigma^2}\mathbf{l}_p^T\mathbf{E}_N\mathbf{E}_N^T\mathbf{l}_p. \quad (17)$$

Therefore, the MUSIC metric $J(p)$ approximates the relative values of time-averaged current intensity $S_{pp}$, and thus it is reasonable to choose the locations of the local maxima of this metric as the locations of the source dipoles.

The spatial filter imaging technique proposed by Robinson *et al.* [29] uses an equation very similar to (9). He has proposed using the weight $\mathbf{w}^T(p) = (\mathbf{l}_p^T\mathbf{D}^{-1})$ to estimate $\hat{f}_p$. That is, the current sources are estimated by using

$$\hat{f}_p(t_k) = \mathbf{l}_p^T\mathbf{D}^{-1}\mathbf{b}(t_k). \quad (18)$$

The difference between (9) and (18) is that (9) contains the scaling term $1/(\mathbf{l}_p^T\mathbf{D}^{-1}\mathbf{l}_p)$. Since this term represents the average squared-intensity, the spatial filter method is effective only when the average current-squared-intensity distribution is considered to be uniform. It may give inaccurate results if there is large nonuniformity.

## V. Conclusion

This paper proposes a method based on the principle of generalized Wiener estimation for obtaining a 3-D biocurrent distribution from spatio-temporal biomagnetic data. The method is formulated under the assumption that current sources are uncorrelated. Computer simulation shows that this method can reconstruct 3-D current distribution where the conventional least-squares minimum-norm method fails. Results of computer simulations taking the influence of noise into account also indicate that a relatively high SNR of more than 20 is needed to implement the proposed method. The calculated point spread function shows that the proposed method has very high spatial resolution, and the pixel interval in the reconstruction must be determined according to the full width at half maximum of the point spread function. The results of computer simulation of the distributed current sources are also presented, including cases where current sources are correlated. The results suggest that the errors due to the source correlation can be small if the correlation is weak.

## Acknowledgment

The authors wish to acknowledge A. Oppelt for the helpful discussion and for his encouragement to proceed this work.

## References

[1] S. J. Williamson and L. Kaufman, "Biomagnetism," *J. Magnetism and Magnetic Mater.*, vol. 22, pp. 129–201, 1981.
[2] M. S. Hämäläinen, and R. J. Ilmoniemi, "Interpreting measured magnetic fields of the brain: Estimates of current distributions," Helsinki Univ. of Technol., Rep. TKK-F-A559, 1984.
[3] J. Z. Wang, S. J. Williamson, and L. Kaufman, "Magnetic source images determined by a lead-field analysis: The unique minimum-norm least-squares estimation," *IEEE Trans. Biomed. Eng.*, vol. 39, pp. 565–75, 1992.
[4] R. Graumann, "The reconstruction of current densities," Helsinki Univ. of Technol., Rep. Biomagnetic Localization and 3-D Modeling, TKK-F-A689, pp. 172–186, 1991.
[5] M. S. Hämäläinen, and R. J. Ilmoniemi, "Interpreting magnetic fields of the brain: Minimum norm estimates," *Med. & Biol. Eng. & Comput.*, vol. 32, pp. 35–42, 1994.
[6] C. W. Crowley, R. E. Greenblatt, and I. Khalil, "Minimum norm estimation of current distributions in realistic geometries," in *Advances in Biomagnetism*, S. J. Williamson *et al.*, Eds. New York: Plenum, 1989, pp. 603–606.
[7] B. Jeffs, R. Leahy, and M. Singh, "An evaluation of methods for neuromagnetic image reconstruction," *IEEE Trans. Biomed. Eng.*, vol. 34, pp. 713–23, 1987.
[8] B. Scholz, K. Sekihara, and R. Killmann, "Lead field reconstruction of biomagnetic current densities in the current supporting planes," in *Proc. 14th Annu. Int. Conf. IEEE Eng. Med. Biol. S.*, Paris, France, Nov. 1992, pp. 2176–2177.
[9] J. Sarvas, "Basic mathematical and electromagnetic concepts of the biomagnetic inverse problem," *Phys. Med. Biol.*, vol. 32, pp. 11–22, 1987.
[10] C. L. Lawson and R. J. Hanson, *Solving Least Squares Problems*. Englewood Cliffs, NJ: Prentice-Hall, 1974.
[11] W. K. Pratt, *Digital Image Processing*. New York: Wiley, 1978.
[12] S. M. Kay, *Fundamentals of Statistical Signal Processing: Estimation Theory*. Englewood Cliffs, NJ: Prentice-Hall, 1993.
[13] W. E. Smith "Estimation of the spatio-temporal correlations of biological electrical sources from their magnetic field," *IEEE Trans. Biomed. Eng.*, vol. 39, pp. 997–1004, 1992.

[14] K. Sekihara and B. Scholz, "The use of noise and signal-source covariance matrices in reconstructing biocurrent distributions from biomagnetic measurements," in *Proc. SPIE Conf. Med. Imag. 1993: Phys. Med. Imag.*, 1993, vol. 1896, pp. 403–411.
[15] ——, "Average-intensity reconstruction and Wiener reconstruction of bioelectric current distribution based on its estimated covariance matrix," *IEEE Trans. Biomed. Eng.*, vol. 42, pp. 149–157, 1995.
[16] S. Schneider, E. Hoenig, H. Reichenberger, K. Abraham-Fuchs, G. Daalmans, W. Moshage, A. Oppelt, G. Röhrlein, H. Stefan, J. Vieth, A. Weikl, and A. Wirth, "Multichannel biomagnetic system for high-resolution functional studies of brain and heart," *Radiol.*, vol. 176, pp. 825–30, 1990.
[17] J. Knuutila and M. S. Hämäläinen, "Characterization of brain noise using a high sensitivity 7-channel magnetometer," in *Proc. 6th Int. Conf. Biomagnet.*, 1987, pp. 186–189.
[18] K. Sekihara, F. Takeuchi, S. Kuriki, and H. Koizumi, "Reduction of brain noise influence in evoked neuromagnetic source localization using noise spatial correlation," *Phys. Med. Biol.*, vol. 39, pp. 937–946, 1994.
[19] A. S. Gevins, S. L. Bressler, N. H. Morgan, B. A. Cutillo, R. M. White, D. S. Greer, and J. Illes, "Event-related covariances during a bimanual visuomotor task. I. Methods and analysis of stimulus- and response-locked data," *Electroenceph. Clin. Neurophysiol.*, vol. 74, pp. 58–75, 1989.
[20] R. Eckhorn, R. Bauer, W. Jordan, M. Brosch, W. Kruse, M. Munk, and H. J. Reitboeck, "Coherent oscillations: A mechanism of feature linking in the visual cortex," *Biol. Cybern.*, vol. 60, pp. 121–130, 1988.
[21] K. J. Friston, C. D. Frith, P. F. Liddle, and R. S. J. Frackowiak, "Functional connectivity: The principal-component analysis of large (PET) data sets," *J. Cereb. Blood Flow Metab.*, vol. 13, pp. 5–14, 1993.
[22] D. Drung, "The PTB 83-SQUID system for biomagnetic applications in a clinic," presented at *Appl. Superconduct. Conf.*, Boston, MA, Oct. 1994.
[23] J. Vrba, B. Taylor, T. Cheung, A. A. Fife, G. Haid, P. R. Kubik, S. Lee, J. McCubbin, and M. B. Burbank, "Noise cancellation by a whole-cortex SQUID MEG system," presented at *Appl. Superconduct. Conf.*, Boston, MA, Oct. 1994.
[24] D. Drung, R. Cantor, M. Peters, P. Ryhänen, and H. Koch "Integrated DC SQUID magnetometer with high $dV/dB$," *IEEE Trans. Magnet.*, vol. 27, pp. 3001–3004, 1991.
[25] S. J. Williamson and L. Kaufman, "Theory of neuroelectric and neuromagnetic fields," in *Auditory Evoked Magnetic Fields and Electric Potentials*, F. Grandori *et al.*, Eds. Basel, Switzerland: Karger, 1990, pp. 1–39.
[26] J. Capon "High-resolution frequency wavenumber spectrum analysis," *Proc. IEEE*, vol. 57, pp. 1408–1419, 1969.
[27] R. O. Schmidt, "Multiple emitter location and signal parameter estimation," *IEEE Trans. Antennas Propagat.*, vol. 34, pp. 276–280, 1986.
[28] J. C. Mosher, P. S. Lewis, and L. Leahy, "Multiple dipole modeling and localization from spatio-temporal MEG data," *IEEE Trans. Biomed. Eng.*, vol. 39, pp. 541–557, 1992.
[29] S. E. Robinson and D. F. Rose "Current source image estimation by spatially filtered MEG," in *Biomagnetism Clinical Aspects*. Amsterdam, The Netherlands: Elsevier Science, 1992, pp. 761–765.

**Kensuke Sekihara** (M'88) received the M.S. degree in 1976 and the Ph.D. degree both from Tokyo Institute of Technology, in 1987.

Since 1976, he has worked with Central Research Laboratory, Hitachi, Ltd., Tokyo, Japan. He was a Visiting Research Scientist at Stanford University, Stanford, CA, from 1985 to 1986, and at Basic Development, Siemens Medical Engineering, Erlangen, Germany, from 1991 to 1992. He is currently a Senior Research Scientist at Hitachi Central Research Laboratory. His research interests include image reconstruction and processing algorithms, biomagnetic inverse problem, statistical estimation theory, and *in vivo* measurements of brain functions.

Dr. Sekihara is a member of IEEE Medicine and Biology Society, Society of Magnetic Resonance, Japanese Society of Biomagnetism, and Japanese Society of Medical Image Processing.

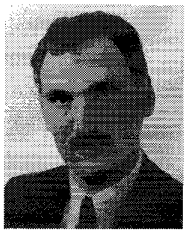

**Bernhard Scholz** received the M.S. degree in 1974 and the Ph.D. degree in 1978, both in physics, from the University of Heidelberg, Germany. His theses were on experimental and theoretical elementary particle physics for the M.S. and Ph.D. degrees, respectively.

After receiving the Ph.D. degree, he worked as an Assistant in theoretical physics. In 1986, he joined the CAD group for VLSI design of the Corporate Research Center of Siemens in Munich, Germany. Since 1987, he has worked in the Simulation Department of the Basic Research Laboratory at the Siemens Medical Engineering Division in Erlangen, Germany. His current research interests are in simulations of complex imaging systems and image reconstruction.